Front. Phys. China (2006) 4: 396－404
DOI 10.1007/s11467-006-0040-x

REVIEW ARTICLE

**ZHANG Xiang-dong**

# Negative refraction and focusing of electromagnetic wave through two-dimensional photonic crystals



**Abstract** The negative refraction of electromagnetic waves in photonic crystals was recently demonstrated experimentally, and the physical properties were analyzed. Microsuperlenses based on two-dimensional photonic crystals were designed and the subwavelength images were observed. In this review, after providing a brief history of the research related to the above phenomena, we will summarize our research works in this field including the method of creating a negative refraction region, generating an absolute negative refraction, the focusing of unpolarized electromagnetic waves, and the effect of interface and disorder on the image by the two-dimensional photonic crystal flat lens. The discussion on the negative refraction and the focusing by high symmetric quasicrystals is also presented.

**Keywords** negative refraction, photonic crystals, focusing, left-handed materials, electromagnetic wave

**PACS numbers** 42.70.Qs, 78.20.Ci, 41.20.Jb, 42.30.Wb

## 1 Introduction

In recent years, there has been a great deal of interest in the study of negative refraction and left-hand materials (LHMs). The properties of such materials were analyzed theoretically by Veselago over 30 years ago [1, 2], but it is only recently that they were demonstrated experimentally [3－5]. As was shown by Vesselago, the LHMs possess a number of unusual electromagnetic effects including negative refraction, inverse Snell's law, a reversed Doppler shift, and a reversed Cerenkov radiation. These anomalous features allow considerable control over light propagation and open the door for new approaches to a variety of applications.

In general, the negative refraction can be created in the following ways. The first is at the interface between a positive conventional medium and a negative refractive metamaterial (such as split-ring resonator) where the electric permittivity and the magnetic permeability are simultaneously negative [1－14]. The second is at the interface of a uniaxially anisotropic medium [15－17]. It has been recently shown that a unique type of interface of a special category of the twinning structures in uniaxial crystals can serve as an example for achieving both negative refraction and total transmission [15－17]. The third is at the interface of the photonic crystal (PC) [18－42]. In this brief review, we will focus our summary on the third way.

## 2 Negative refraction and image by two-dimensional photonic crystal

Negative refraction in photonic crystals was first observed by Kosaka *et al*. in 1998 [18]. After which there have been a number of reported experimental demonstrations and theoretical studies in this field [19－42]. The physical principles that allow for a negative refraction in the PC arise from the dispersion characteristics of wave propagation in a periodic medium, which can be well described by analyzing the equifrequency surface (EFS) of the band structures [19－42]. Figure 1 represents a typical branch of a dispersion surface in reciprocal space for a PC. The curvature of the dispersion surface turns from downward to upward, and the incident light comes from the top of the figure. The direction of propagation of the light in the PC is normal to the dispersion surface. Due to the different shape of the curvature, the flux directions of the propagation wave at various points are different, which can be obtained by the group velocity,

ZHANG Xiang-dong (✉)
Department of Physics, Beijing Normal University, Beijing 100875, China
E-mail: zhangxd@bnu.edu.cn

*Received August 28, 2006*

$v_g = \nabla_k \omega(k)$, where $\omega$ is the optical frequency at the wave vector $k$. This means that there are various transport properties of the wave in the PCs, for example, divergent propagation as in a concave lens (point $A$), collimated propagation (point $B$) and negative refraction (point $C$). That is to say, the negative refraction is only one way for transmitting waves in the PC. The refraction is determined by the shape of the EFS or the structure of the PC allowing us to regulate it by choosing the various structures of the PC.

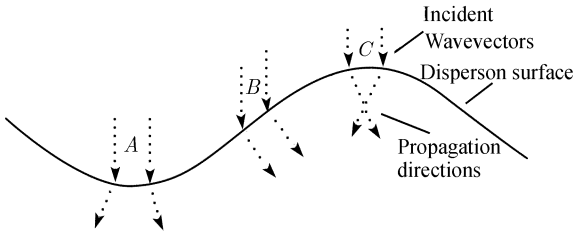


**Fig. 1** A schematic illustration of wave transmitting through the PC. Arrows above the dispersion surface indicate incident wave vectors in reciprocal space. Arrows below the dispersion surface indicate the energy flow in real space.

Figure 2 describes several constant frequency contours for the second band of a two-dimensional (2D) PC with a triangular lattice for the S wave. It is clear from the figure that the frequencies increase inwards, meaning that $\boldsymbol{S}\cdot\boldsymbol{k} < 0$ and the group velocities $v_g$ are opposite of the phase velocity. Here, $\boldsymbol{S}$ and $\boldsymbol{k}$ represent the Poynting vector and wave vector, respectively. This indicates that the transmitting features of the wave in such a PC structure have left-handed behavior. At the same time, we also notice that some EFS contours such as $\omega = 0.42 - 0.47(2\pi a/c)$ are very close to a perfect circle, indicating that the crystal can be regarded as an effective homogeneous left-handed medium at these frequencies.

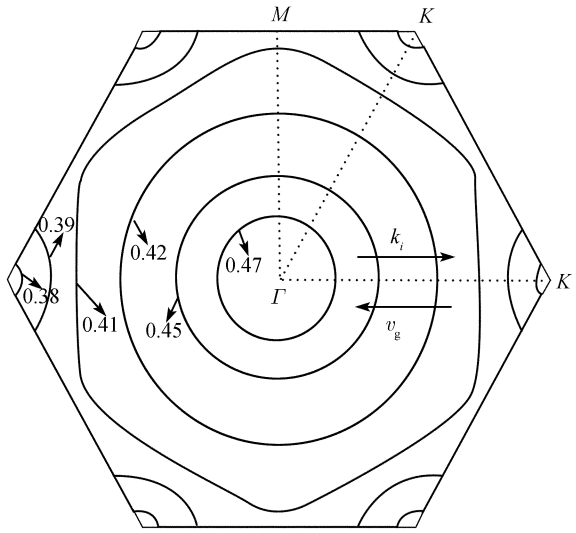


**Fig. 2** Several constant frequency contours for the second band of the 2D PC with a triangular lattice of coated cylinder in air for the S wave. The radii of the dielectric cylinder and inner metallic cylinder are $R = 0.45\ a$ and $r = 0.25\ a$, respectively.

The above example shows that the maximum dispersion curve is located at the $\Gamma$ point of the Brillouin zone and the negative refraction comes from the backward wave effect. In fact, the negative refraction can also be realized without employing the backward wave effect [22—33]. Figure 3 displays several constant frequency contours for the first band of the 2D PC with a square lattice for the S wave. We find that the lowest bands have $\boldsymbol{S}\cdot\boldsymbol{k} > 0$ everywhere within the first Brillouin zone, meaning that the group velocities are never opposite to the phase velocity. However, some low frequency contours such as 0.232 are significantly distorted from a circle, which are convex around $M$ points. The conservation of the $k$ component along the surface of refraction will also result in the negative refraction effect in this case. The advantages of a negative refraction in the lowest valence band are that it has a single-mode and has high transmission. At high frequency, the left-handed and the right-handed behaviors are generated simultaneously due to the excitations of the multiple-mode, which has been pointed out in Ref. [21]. The single-mode and all-angular negative refraction are very important to some applications in designing optical devices, which will be introduced in the following.

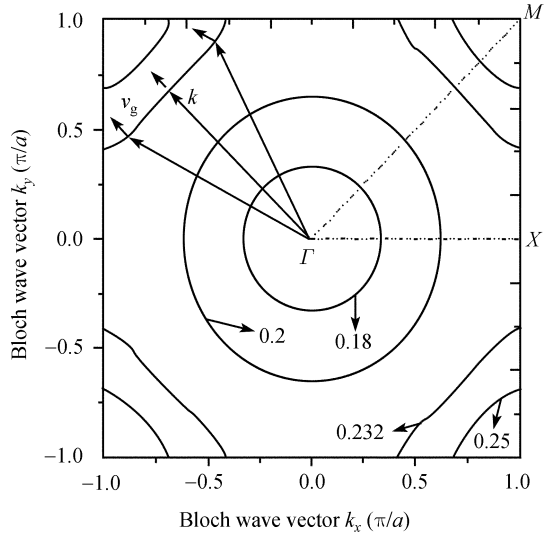


**Fig. 3** Several constant frequency contours for the first band of the 2D PC with a square lattice of coated cylinder in air for the S wave. The radii of the dielectric cylinder and inner metallic cylinder are $R = 0.45\ a$ and $r = 0.15\ a$, respectively.

The two seemingly different situations do share a common feature, that is, the photonic effective mass near a local maximum of the dispersion curve is negative-definite. The negative refraction at both high and low frequencies rely on the same mechanism that the relative wave vector of a local frequency maximum is pointed opposite to the group velocity. The two have the same usefulness. for example, they both can be applied to design a flat lens and realize the focusing of the wave. It is well known that an important application of negative refraction materials is the flat lens. Ideally, a flat lens can focus a point source on one side of the

lens into a real point image on the other side even for cases of a parallel sided slab of material. It has advantages over conventional lenses, for example, it can go beyond the traditional limitation on lens performance and focus light on to an area smaller than a square wavelength.

Figure 4 represents a typical field intensity pattern for the S wave across the flat lens consisting of 2D PCs with a triangular lattice. The structure and parameters of the PC correspond to those in Fig. 2. $X$ and $Y$ represent the vertical and transverse direction of the propagating wave, respectively. The field intensity in the figure is over a $30a \times 30a$ region around the center of the sample. The geometry of the PC slab is also displayed for a clear view. The high quality image in the opposite side of the slab and the focusing in the middle of the slab are clearly observed. If we move the position of the source, the image distance changes simultaneously. The relation between the object length and the image distance explicitly follows the well-known wave-beam negative refraction law. This means that the image is non-near-field. This theoretical result has been demonstrated experimentally by us [42].

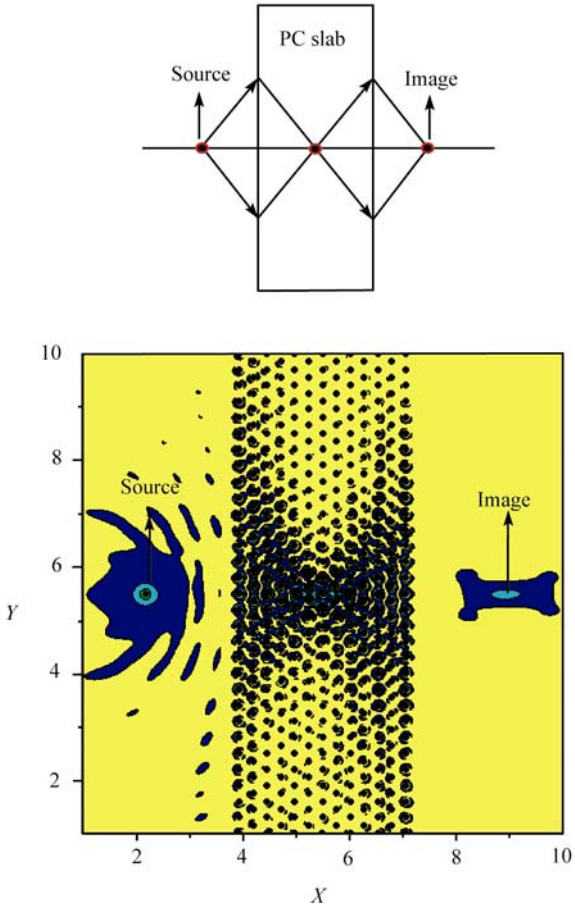


**Fig. 4** The intensity distributions of point source and its image across a $11a$ 2D PC slab at $\omega = 0.42\,(2\pi a/c)$ for the S wave. The structure and parameters are identical with those in Fig. 2. Schematic picture depicting the lensing of a source by a PC slab to an image are shown on top of the figure.

In contrast to the result in Fig. 4, Fig. 5 describes a case with a square lattice. The structure and parameters correspond to those in Fig. 3. In such a case, the position of the image does not change with the moving of the source, and the image is located at the near-field region. The difference between Fig. 4 and Fig. 5 had led to some argument about the origin of the focusing. Some authors think that the focusing arises from the self-collimation effect instead of the all-angle negative refraction (AANR) for such a case [29, 33]. The argument has been recently clarified by us and Hu *et al*. [36, 37]. We will give the detailed introduction in the next Section.

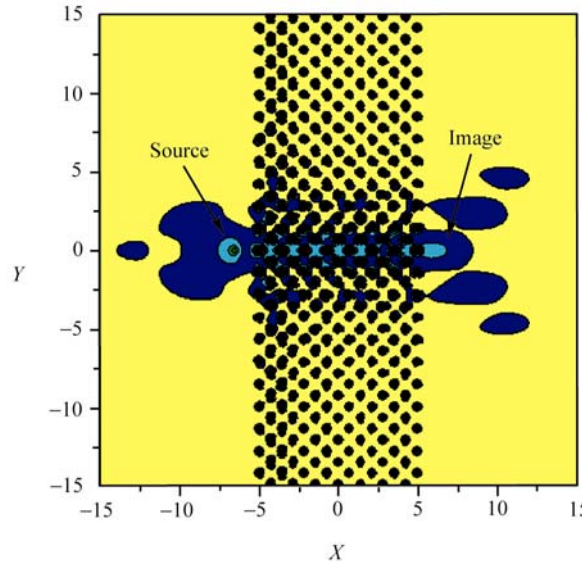


**Fig. 5** The intensity distributions of a point source and its image across a $11a$ 2D PC slab at $\omega = 0.231\,(2\pi a/c)$. The structure and parameters are identical with Fig. 2.

## 3 Creating negative refraction by tuning the scatters

In fact, the AANR and the high transmission are very important to the design of a microsuperlens and for wave focusing. However, the AANR region is usually narrow or absent in some 2D PC structures. Thus, the creation and enlargement of the AANR region becomes an important issue. Recently, we have presented a method to create and enlarge the AANR region by using insertion [30]. Consider a 2D square lattice of dielectric cylinders immersed in the air background with the lattice constant a. The radius and the dielectric constant of the cylinders are $0.45a$ and 14, respectively. The band structures of this system are shown in Fig. 6 (a). The AANR region does not exist in this case. However, the situation can be changed by introducing a metallic component in the center of every dielectric cylinder, resulting in a "coated cylinder" PC. The corresponding photonic band structures with an inner metal core $r$ = 0.25 $a$ is plotted in Fig. 6 (b). The AANR region appears, which has been marked by dark shadow. Within this region, the EM beam

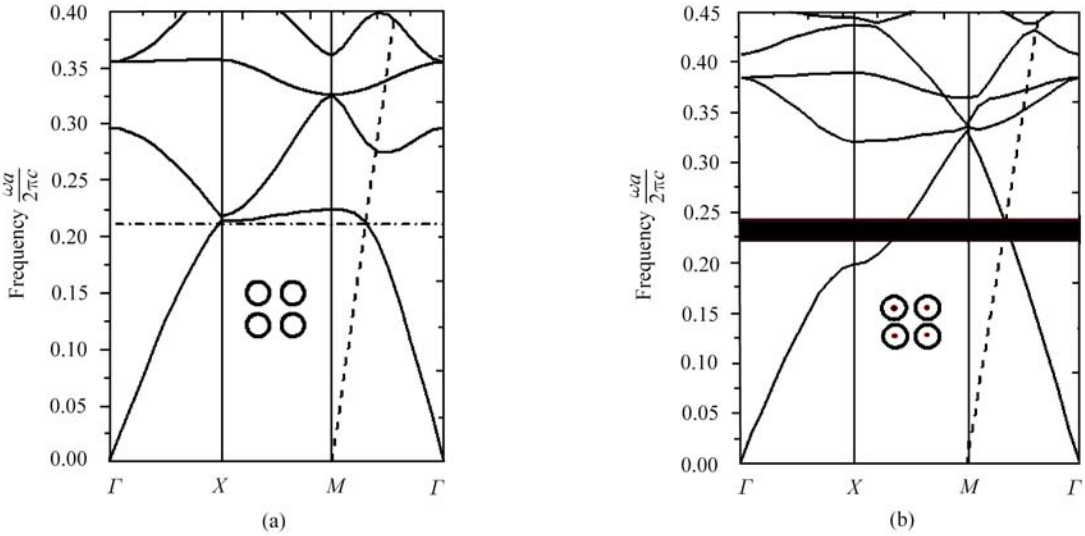


**Fig. 6** **(a)** The calculated photonic band structures of a square lattice of dielectric cylinders with radius $R$ = 0.45 $a$ and $\varepsilon = 14$ in the air for P wave. **(b)** The corresponding case for coated cylinders with inner metallic cylinder radius $r$ = 0.25 $a$. The insets show the microstructures. The light line shifted to $M$ is shown by dashed lines.

incident on the $\Gamma M$ surface with different incident angles will couple to a single Bloch mode that propagates into this crystal on the negative side of the boundary normal.

It is interesting that the AANR region cannot only be created and enlarged by introducing a metallic component in the center of every dielectric cylinders, the focusing feature by such a PC slab can also be regulated by the size of the inner metal core. In Fig. 5, we have shown that focusing is only located at the near-field region by the PC slab with a square lattice for the lowest valence band due to the anisotropy of the dispersion (or the self-collimation effect). However, the self-collimation effect can in principle be suppressed by changing the scatter, and the position of the focusing (in near-field region or non-near-field region) can be regulated. Figure 7 (a) shows the intensity distributions of the point source and its image across an 11$a$ 2D PC slab with an inner metal core $r$ = 0.25 $a$ at $\omega = 0.245\,(2\pi a / c)$. Comparing it with Fig. 5, we find that the image distance becomes larger and the position of the focusing can move with the object distance, although it does not satisfy the negative refraction law. If we continue to increase the size of the metal core such as $r$ = 0.43 $a$, the focusing based on the negative refraction law has been realized. Figure 7 (b) represents such a case. The position of the focusing depends on the shape of the EFS. This means that the focusing in the near-field region or the non-near-field region, all come from negative refraction.

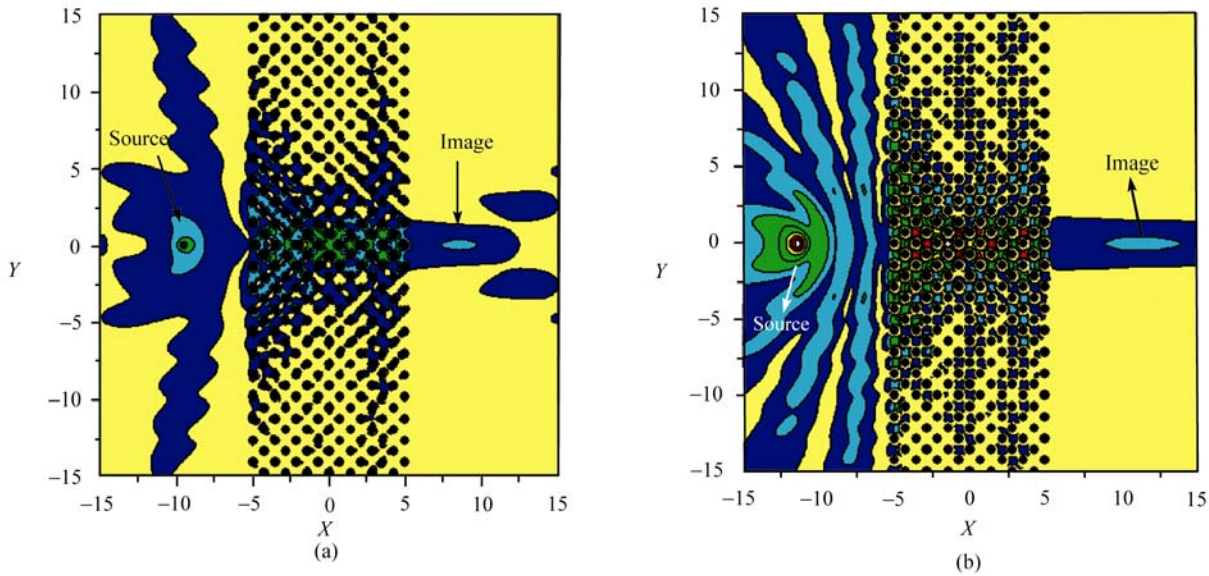


**Fig. 7** The intensity distributions of point source and its image across an 11$a$ 2D PC slab with inner metal core $r$ = 0.25 $a$ at $\omega = 0.245\,(2\pi a / c)$ **(a)**, with inner metal core $r$ = 0.43 $a$ at $\omega = 0.317\,(2\pi a / c)$ **(b)** for the P wave. The structure and parameters of the PC are identical to those in Fig. 6.

## 4 Absolute negative refraction and imaging of unpolarized electromagnetic waves

It is well known that an electromagnetic wave can decompose into $E$ polarization (S wave) and $H$ polarization (P wave) modes for the 2D PC structures. However, the previous discussions about the negative refraction and the focusing of the wave in the 2D PC all focused on a certain polarized wave, S wave or P wave. It is a natural question to ask whether or not a complete negative refraction region for all polarized waves exists. Recently, our studies have shown that such a region exists [31, 39]. It is interesting that such a phenomenon can be engineered by using a perturbation method [39].

Figures 8 (a) and (b) represent the photonic band structures of a triangular lattice of coated cylinder in air for the S wave and the P wave, respectively. The relative refractive index of $n = -1$ for the S wave at $\omega = 0.49\,(2\pi a/c)$ and the P wave at $\omega = 0.44\,(2\pi a/c)$ have been marked by dotted lines. We find that the same structure and parameters yield $n = -1$ at different frequency for both types of polarizations. In fact, such a case can be changed by adding a component to the existing photonic crystal. The dielectric properties of such a component are chosen according to the field-energy distribution of Bloch states at the band edges. Thus, we calculate the field-energy distribution of the band-edge state in a unit cell. For the $2\Gamma$ point of the S wave in Fig. 8 (a), the absolute value of the electric field distribution outside the cylinder in a Wigner unit cell is plotted in Fig. 9 (a). It is shown that the electric field at the six symmetric points of a Wigner unit cell is large. If we choose a dielectric material to insert at the positions of these points, the field distribution in the unit cell will change, which leads to the shift of the band edge. The shift tendency and range for the S wave can be estimated by the following perturbation formula,

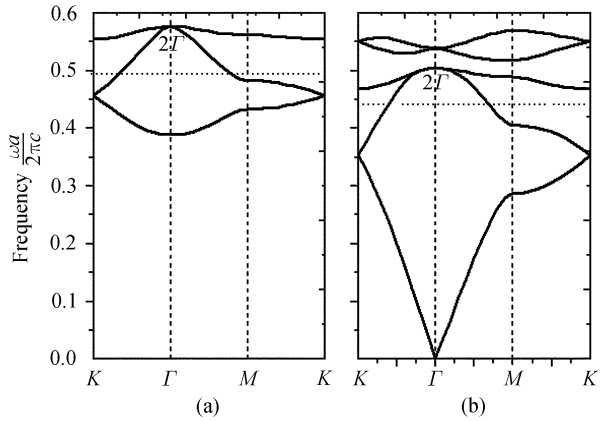


**Fig. 8** The calculated photonic band structures of a triangular lattice of coated cylinder in air for **(a)** S wave and **(b)** P wave. The radii of the dielectric cylinder is $R = 0.4\ a$. The inner metallic cylinders are $r = 0.25a$ for both polarized waves. The dielectric constants are $\varepsilon = 12.96$. Dotted lines vs. the frequencies with negative refraction index of −1.

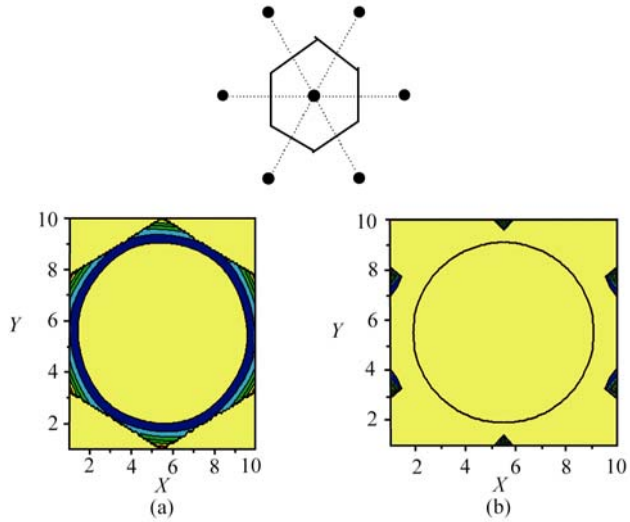


**Fig. 9** **(a)** The distribution of the absolute value of the electric field outside the cylinder (in arbitrary units) at the band edge $2\Gamma$ in the Wigner unit cell for the S wave. **(b)** The distribution of the absolute value of the displacement field outside the cylinder (in arbitrary units) at the band edge in the Wigner unit cell for the P wave. The corresponding Wigner unit cell is plotted on the top of the figure.

$$\left(\frac{\tilde{\omega}_{nk}}{\omega_{nk}}\right)^2 - 1 \approx \frac{\int [\tilde{\varepsilon}^{-1}(\boldsymbol{r}) - \varepsilon^{-1}(\boldsymbol{r})]\,|\,\boldsymbol{D}_{nk}(\boldsymbol{r})\,|^2\ \mathrm{d}\boldsymbol{r}}{\int \varepsilon^{-1}(\boldsymbol{r})\,|\,\boldsymbol{D}_{nk}(\boldsymbol{r})\,|^2\ \mathrm{d}\boldsymbol{r}} \tag{1}$$

Here, $\tilde{\varepsilon}(\boldsymbol{r})$ and $\tilde{\omega}_{nk}$ represent the new dielectric constant and the eigenfrequency, respectively, corresponding to the original $\varepsilon$ and $\omega_{nk}$. The function $\tilde{\varepsilon}(\boldsymbol{r}) - \varepsilon(\boldsymbol{r})$ is nonzero, only at the insertion position. The shift tendency and range of the band edge depend on the dielectric properties of the additional components as well as the field-energy distribution at the band edge. For example, if we choose to insert the dielectric cylinders, we can deduce that the band edge shifts down. With the change of the band structure, the negative refraction region will change at the same time.

Similar to the above case of the S wave, for the P wave, when the new components are inserted into the unit cell, the frequency shift can also be estimated by the following relation

$$\left(\frac{\tilde{\omega}_{nk}}{\omega_{nk}}\right)^2 - 1 \approx \frac{\int [\varepsilon(\boldsymbol{r}) - \tilde{\varepsilon}(\boldsymbol{r})]\,|\,\boldsymbol{E}_{nk}(\boldsymbol{r})\,|^2\ \mathrm{d}\boldsymbol{r}}{\int \varepsilon(\boldsymbol{r})\,|\,\boldsymbol{E}_{nk}(\boldsymbol{r})\,|^2\ \mathrm{d}\boldsymbol{r}} \tag{2}$$

Here $\boldsymbol{E}_{nk}(\boldsymbol{r})$ represents the displacement field in the unit cell. The intensity distribution of the displacement field outside the cylinder in a Wigner unit cell at the $2\Gamma$ point of the P wave in Fig. 8 (b) is plotted in Fig. 9 (b). We find that the displacement field at six symmetric points of a Wigner unit cell is also large. If we choose the same dielectric components to insert the same positions in the unit cell for the P wave as the case of the S wave, the drop of the frequency at the $2\Gamma$ point can also be found. However, the shift for the P wave is smaller than that of the S wave. Therefore, it is pos-

sible to obtain the same effective refractive index for both polarized waves by choosing a suitable dielectric component to insert. For example, when the dielectric cylinders with $R$ = 0.11 $a$ and $\varepsilon = 12.96$ are inserted, the frequency positions with relative refractive index of −1 become $\omega = 0.405(2\pi a/c)$ for the S and the P waves at the same time. That is to say, the same structure yields $n$ = −1 at the same frequency for both polarized waves.

The above theoretical analyses have been demonstrated by exact numerical calculation [39]. The calculated results of the negative refraction indexes as a function of the frequency are plotted in Figs. 10 (a) and (b). Figures 10 (a) and (b) correspond to the cases before and after the insertion, respectively. The solid lines correspond to the S wave and the dotted lines to the P wave. It can be seen clearly that the positions of effective refractive index of $n$ = −1 for the S and P waves in the original system are different. However, the cross point of an effective refractive indexes of $n$ = −1 for the S and P waves appears at $\omega = 0.405(2\pi a/c)$ after the dielectric cylinders with $R$ = 0.11 $a$ and $\varepsilon = 12.96$ are inserted. Thus the focus of unpolarized electromagnetic waves can be realized by the flat lens consisting of such a modified PC.

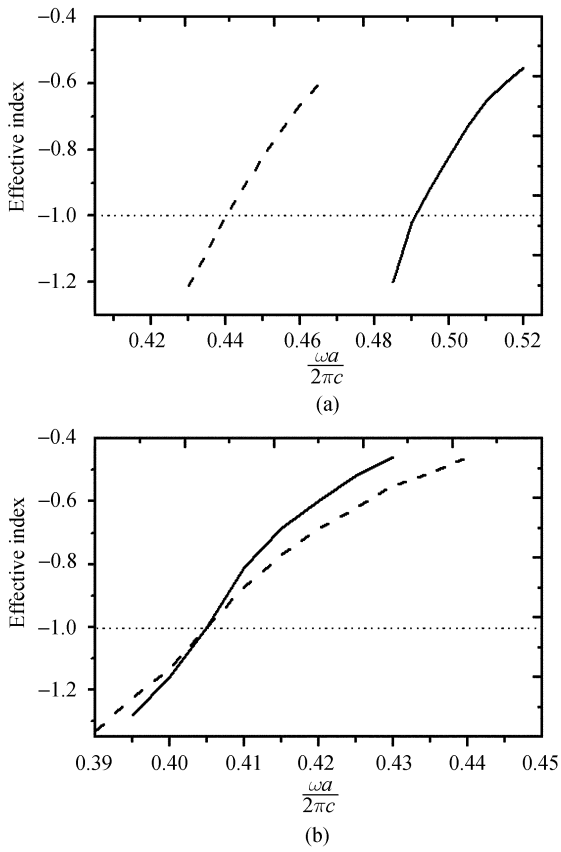


**Fig. 10** Effective indexes vs frequencies **(a)** before and **(b)** after the additional components are inserted. The solid lines and dashed lines correspond to the S wave and the P wave, respectively. The positions of relative refractive index of −1 are marked by dotted lines.

## 5 Effect of interface and disorder on the image by two-dimensional photonic crystal flat lens

There are two aspects relating to image and focusing. One is position (in near-field region or non-near-field region), and the other is resolution (full width at half maximum of the focus spot). The position of the image depends on the effective refractive index n of the sample and the homogeneity of the materials. In the case where $n$ = −1 and the transmission is single-mode, the imaging behavior depends on the slab thickness and the object distance, explicitly following the wave-beam negative refraction law, which has been discussed above. However, due to the anisotropy of dispersion in some 2D PCs, the refraction angles are not linearly proportional to the incident angles when a plane wave is incident from the vacuum to the PC. This is the reason why only the near-field images were observed in some works [22—40]. The position of the image does not depend on whether or not the evanescent waves are amplified. That is to say, the focus and image can still be observed if only the propagating waves are considered. In such a case, the image resolution cannot beat the diffraction-limit. In contrast, the superlensing effect comes from the evanescent waves (or resonance transmission). The excitation of the surface mode (or the appearance of resonant transmission) can improve the image resolution [25, 40]. In this part, we discuss the effect of interface and disorder on the image.

Based on the theoretical analysis of Ref. [2], the perfect lens consists of a homogeneous LHM with $n$ = −1 that can focus a point source on a perfect image without any loss of reflection. However, for the photonic-crystal-based flat lens, even in cases with an effective index $n$ = −1, the loss of reflection is inevitable due to the scattering on the interface layers. This has been demonstrated in the discussion above [19—42]. A few works [25] have shown that the surface termination within a specific cut of the structure can excite the surface waves and allow the reconstruction of the evanescent waves for a better focus. In fact, apart from the surface termination, the other methods such as changing the dielectric constants of the interface layers, adding symmetric cap layers and introducing optical gain in the surface layers can also improve the image resolution [40].

Figures 11(a) and (b) display the comparative results between the unmodified and the modified cases by adding the symmetric cap layers; (a) corresponds to the field intensity distributions along the vertical $X$ direction at $Y$ = 0.0 and (b) to the transverse $Y$ direction at the image plane for the S wave point source across the PC slab with the cap layers. Comparing the unmodified results (*solid lines*) with those modified results (*dotted lines*), we find that the intensities of the central peaks increase, whereas the transverse half-widths decrease.

The cap layers can be added in various ways. In Fig. 11, we only consider the cap layers consisting of dielectric cylinders with $R$ = 0.4 $a$. The lattice constants and the positions

of the cylinders on the cap layers correspond to the PC slab. That is to say, the thickness of the PC slab increases by 2 $a$, and at the same time the coated cylinders on two surface layers are replaced by the dielectric cylinders with $R = 0.4a$. We have to point out that the improvement of the image resolution by the cap layers cannot be realized in any case, except for the appearance of the resonance [40]. Dotted lines in Fig. 11 describe such a case. Similar to adding symmetric cap layers, changing the dielectric constants of interface layers can also lead to the appearance of such a phenomenon [40].

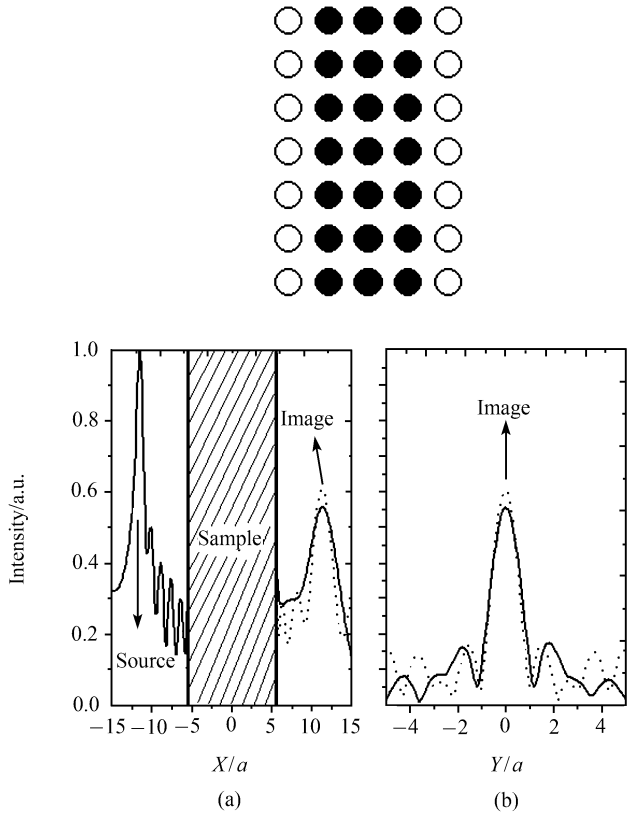


**Fig. 11** Intensity distributions along the vertical $X$ direction at $Y = 0.0$ **(a)** and the transverse $Y$ direction at the image plane **(b)** for P wave. Solid lines represent the unmodified cases. Dotted line corresponds to the case with $R = 0.4\ a$ and $\varepsilon = 4.5$ dielectric cylinder cap layers. The crystal and parameters are identical to those in Fig. 8. Schematic picture is shown on the top.

In contrast to the improvement of the image resolution by tuning the surface structure, the effect of disorder always reduces the image resolution (including image peaks and full width at half maximum of the focusing). The role of the disorder is similar to that of material absorption, which has been discussed in Ref. [40].

## 6 Negative refraction and focusing by high symmetric quasicrystals

It is evident that the anisotropy of the dispersion is dependent on the symmetry of the PC lattice. In order to obtain a homogeneous dispersion and realize the non-near-field focus, we should use the structures with a high symmetry to construct the flat lens. However, the highest level of symmetry that can be found in a periodic lattice is six. In contrast, the highest symmetry in a photonic quasicrystals (PQCs) can reach 12. The problem is whether or not negative refraction exists in these PQCs. If it exists, what kind of properties does it possess? Based on these problems, we have performed a detailed investigation on the phenomenon of negative refraction in the PQCs [43]. The problems have been clarified.

Depending on the level of the symmetry [44,45], the PQCs can be divided into 5-fold, 8-fold, 10-fold and 12-fold structures. Figures 12 (a) and (b) describe two kinds of structures with a 12-fold symmetry. The PQC structures with an 8-fold and a 10-fold symmetry are shown in Figs. 12 (c) and (d), respectively.

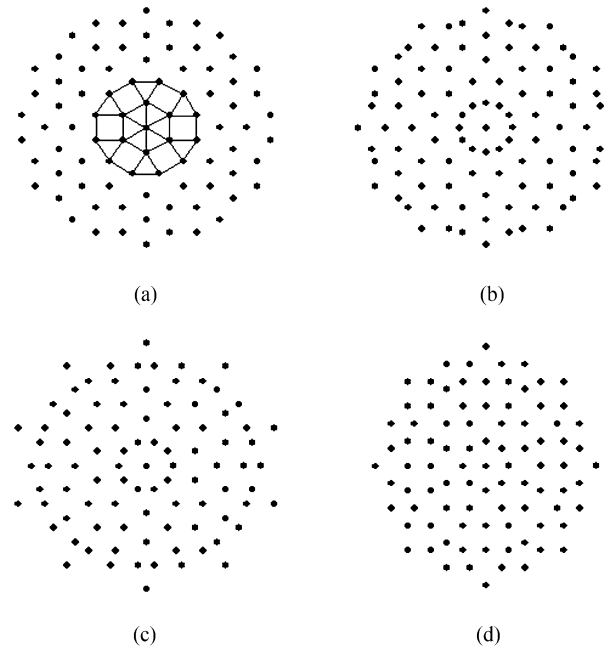


**Fig. 12** Schemes of the basic quasicrystal structures. **(a)** 12-fold quasicrystal with a random square-triangle tiling system. **(b)** 12-fold quasicrystal with a general rotated symmetry. **(c)** 10-fold quasicrystal. **(d)** 8-fold quasicrystal.

The 12-fold PQC based on a random square-triangle tiling system [Fig. 12 (a)] is first considered both theoretically and experimentally [43]. The samples, consisting of a number of dielectric cylinders embedded in a styrofoam template, have been fabricated experimentally. The transmission intensity as a function of refractive angle has been measured. The existence of the negative refraction has been shown [43].

The origin of the negative refraction in such a PQC can be understood similar to the cases in the periodic PCs. Some experiments [46] have shown that analogous concepts to

Bloch functions and to Bloch-like states in the periodic structures can be applied to some PQCs. In particular, the 12-fold PQC is composed of two basic units (triangle and square) tiling together. One is convinced that each unit, when arranged in a periodic lattice, can generate a negative refraction. If we bring the triangle and square together into a PQC, a negative refraction phenomenon is expected.

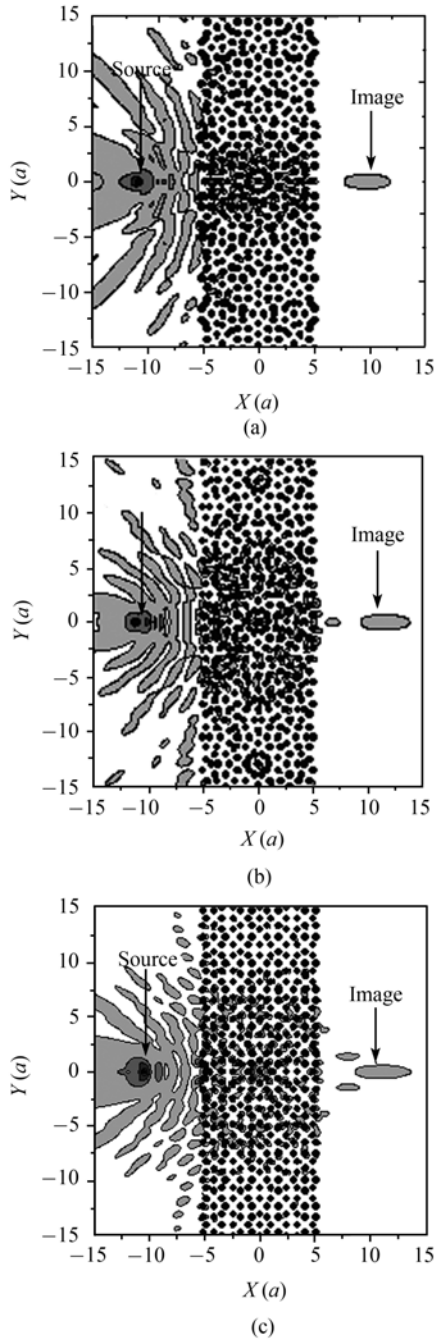


**Fig. 13** The intensity distributions of point sources and their images across the 11*a* 2D PQC slabs. **(a)** 12-fold PQC [Fig. 12 (b)]. **(b)** 10-fold PQC [Fig.12(c)]. **(c)** 8-fold PQC [Fig. 12 (d)].

In fact, the negative refraction not only exists in the random square-triangle tiling system, it also exists in other high-symmetry PQC. Similar to the periodic PC, we can also use the PQC to design the flat lens and realize the focusing of the wave. Figures 13 (a), (b) and (c) describe the flat lenses and the focusing by a 12-fold [Fig. 12 (b)], a 10-fold [Fig. 12 (c)] and an 8-fold [Fig. 12 (d)] PQC, respectively. The thicknesses of the slabs are taken as 11*a*. The continuous-wave point sources are placed at a distance of 5.5*a* (half thickness of the sample) from the left surface of the slab. The frequencies of the incident wave emitting from the point sources are $\omega$ = 0.4365, 0.4367 and 0.436 ($2\pi c/a$) for the three kinds of PQCs, respectively. The non-near-field focuses in the opposite sides are observed for all cases. It is interesting that the focuses are not only for the S wave, but are also for the P wave at the same time. Our calculated results indicate that the high symmetry PQC slabs possess a universal feature for the non-near-field focus of two kinds of polarized waves. That is to say, the PQC slabs can focus the unpolarized wave emitting from a point source at the approximately same frequency. Such a superior feature originates from a high rotational symmetry and negative refraction, which they posses [43].

We would like to point out that the PQCs are not better than the periodic PC in all aspects. However, the PQC has some advantages in producing non-near-field images due to their higher rotational symmetry. For example, it is very difficult to construct a flat lens by using a pure dielectric cylinder of periodic structure to realize the non-near-field focus for the S wave, but it is easy to complete using a high symmetry PQC slab as has been shown. Thus, this investigation on the negative refraction and the focusing of the PQC can now open a new window in the realistic application of such a phenomenon.

## 7 Summary

Based on a series of our researches, in this paper we have offered a concise account of the history of research related to negative refraction and the focusing of electromagnetic wave through 2D photonic crystals. The physical principles causing such a phenomenon have also been analyzed. The different kinds of focusing by 2D PC slabs have been summarized. In particular, the methods to create and enlarge the negative refraction region have been introduced. The realization of an absolute negative refraction and the focusing of unpolarized electromagnetic waves have also been reviewed. The effects of interface and disorder on the image of a 2D PC flat lens have been discussed. The investigations on the negative refraction and the focusing by high symmetric PQC have also been presented.

**Acknowledgements** This work was supported by the National Key Basic Research Special Foundation of China (Grant No. 2001CB610402) and the National Natural Science Foundation of China (Grant No. 10374009). The project was supported by Program for New Century Excellent Talents in University (NCET) and the Research Fund for the Doctoral Program of-Higher Education (RFDP).

## References


1. Veselago V. G., Sov. Phys. Usp., 1968, 10: 509
2. Pendry J. B., Phys. Rev. Lett., 2000, 85: 3966
3. Shelby R. A., Smith D. R., and Schultz S., Science, 2001, 292: 77
4. Smith D. R., Padilla W. J., View D. C., Nemat-Nasser S. C., and Schultz S., Phys. Rev. Lett., 2000, 84: 4184
5. Smith D. R. and Kroll N., Phys. Rev. Lett.,2000, 84: 2933
6. Markos P. and Soukoulis C. M., Phys. Rev. E, 2002, 65: 036622; Phys. Rev. B, 2002, 65: 033401
7. Pacheco J., Jr., Grzegorczyk T. M., Wu B. L., Zhang Y., and Kong J. A., Phys. Rev. Lett., 2002, 89: 257401
8. Marques R., Martel J., Mesa F., and Medina F., Phys. Rev. Lett. ,2002,89: 183901
9. 9. Foteinopoulou S., Economou E. N., and Soukoulis C. M., Phys. Rev. Lett., 2003, 90: 107402
10. Smith D. R. and Schurig D., Phys. Rev. Lett., 2003, 90: 077405
11. Houck A. A., Brock J. B. and Chuang I. L., Phys. Rev. Lett., 2003, 90: 137401
12. Parazzoli C. G., Greegor R. B., Li K., Koltenbah B. E. C., and Tanielian M., Phys. Rev. Lett., 2003, 90: 107401
13. Grbic A. and Eleftheriades G. V., Phys. Rev. Lett., 2004, 92: 117403
14. Chen L., He S., and Shen L., Phys. Rev. Lett., 2004, 92: 107404
15. Zhang Y., Fluegel B., and Mascarenhas A., Phys. Rev. Lett., 2003, 91: 157404
16. Liu Z., Lin Z., and Chui S. T., Phys. Rev. B, 2004, 69: 115402
17. Zhang X., Appl. Phys. Lett., 2006, 88: 052114
18. Kosaka H., Kawashima T., Tomita A., Notomi M., Tamamura T., Sato T., and Kawakami S., Phys. Rev. B, 1998, 58: 10096
19. Notomi M., Phys. Rev. B, 2000, 62: 10696
20. Gralak B., Enoch S., and Tayeb G., J. Opt. Soc. Am. A,2000, 17: 1012
21. Foteinopoulou S. and Soukoulis C. M., Phys. Rev. B, 2003, 67: 235107
22. Luo C., Johnson S. G., Joannopoulos J. D.and Pendry J. B., Phys. Rev. B, 2002, 65: 201104
23. Luo C., Johnson S. G., Joannopoulos J. D. and Pendry J. B., Opt. Express, 2003, 11: 746
24. Luo C., Johnson S. G. and Joannopoulos J. D., Appl. Phys. Lett., 2002, 83: 2352
25. Luo C., Johnson S. G., Joannopoulos J. D. and Pendry J. B., Phys. Rev. B, 2003, 68: 045115
26. Cubukcu E., Aydin K., Ozbay E., Foteinopoulou S., and Soukoulis C. M., Nature (London), 2003, 423: 604
27. Parimi P. V., Lu W. T., Vodo P., and Sridhar S., Nature, 2003, 426: 404
28. Cubukcu E., Aydin K., Ozbay E., Foteinopoulou S., and Soukoulis C. M., Phys. Rev. Lett., 2003, 91: 207401
29. Li Z. Y. and Lin L. L., Phys. Rev. B, 2003, 68: 245110
30. Zhang X., Appl. Phys. Lett., 2005, 86:, 121103
31. Zhang X., Phys. Rev. B, 2004, 70: 205102
32. He S. L., Ruan Z. C., Chen L., and Shen Jianqi, Phys. Rev. B, 2004, 70: 115113
33. Belov P., Simovski C., and Ikonen P., Phys. Rev. B, 2005, 71: 193105
34. Wang X., Ren Z. F., and Kempa K., Optics Express, 2004, 12: 2919
35. Wang X., Ren Z. F., and Kempa K., Phys. Rev. B, 2005, 71: 085101
36. Hu X. and Chan C. T., Appl. Phys. Lett., 2004, 85: 1520
37. Zhang X., Phys. Rev. E, 2005, 71: 037601
38. Zhang X., Phys. Rev. B, 2004, 70: 195110
39. Zhang X., Phys. Rev. B, 2005, 71: 235103
40. Zhang X., Phys. Rev. B, 2005, 71: 165116
41. Berrier A., Mulot M., Swillo M., Qiu M., Thylen L., Talneau A., and Anand S., Phys. Rev. Lett., 2004, 93: 073902
42. Feng Z., Zhang X., et. al., Phys. Rev. B, 2006, 73: 075118
43. Feng Z., Zhang X., Wang Y.Q., Li Z.Y., Cheng B.Y., and Zhang D.Z., Phys. Rev. Lett., 2005, 94: 247402
44. Zhang X., Zhang Z. Q., and Chan C. T., Phys. Rev. B, 2001, 63: 081105
45. Jin C., Cheng B., Man B., Li Z., Zhang D. Z., Ban S., and Sun B., Appl. Phys. Lett., 1999, 75: 1848
46. Rotenberg E., Theis W., Horn K., and Gille P., Nature (London), 2000, 406: 602